UNIVERSITÄT FÜR BODENKULTUR WIEN
University of Natural Resources
and Life Sciences, Vienna

Final research report

Intrinsic fluorescence changes associated with the structural changes of proteins and their effects on the coalescence of protein adhesives

submitted by

Stefanie KORNFELD, BSc

Madison, 02 2024

Supervisor:

Univ.Prof. Dipl.-Ing. Dr. Johannes Konnerth
Institute of Wood Technology and
Renewable Materials
Department of Material Sciences and
Engineering (MAP)

Co-Supervisor:

Christopher G. Hunt, PhD
Forest Products Laboratory
United States Department of
Process Agriculture
Department of the US government

The beautiful thing about learning is that

no one can take it away from you.

B.B. King

Acknowledgments

First, I would like to extend my heartfelt thanks to my supervisor, Johannes Konnerth for not only encouraging my pursuit of a Master's thesis in the USA but also facilitating the connection with Christopher G. Hunt. His support over the years has been extremely valuable in shaping my academic journey. Additionally, I would like to express profound thanks to Hendrikus Wilhelmus Gerardus Van Herwijnen. His decision to hire me as a student worker at Wood K plus, coupled with his support over several years, has been invaluable. Working alongside him has been a rewarding experience.

I extend my deepest gratitude to Christopher G. Hunt. His guidance and several discussions on my Master's thesis were extremely helpful, and I equally appreciate his exceptionally warm hospitality and the shared experiences that enriched my research stay. Special thanks go to Nayomi Plaza Rodriguez for introducing me to Python and for her many suggestions and help in analyzing DLS and MALS data. Furthermore, I would like to acknowledge Linda F. Lorenz for her contributions, including the testing of ABES samples. My sincere thanks also extend to Carl J. Houtman for providing insightful explanations on diverse subjects and helping with technical issues.

I also want to express my deepest gratitude to the Marshall Plan Foundation for their generous financial support, which made my research stay in Madison possible.

Finally, to my friends in Austria, especially Sabi and Meli, I appreciate their ongoing support. Likewise, I extend my thanks to my boyfriend Herman, my brother Daniel, and my parents for their constant presence and encouragement throughout my life.

Table of content

Abstract

Sustainable protein-based adhesives have difficulties competing with petroleum-based adhesives due to their limited wet strength and higher production costs. In this study, we investigated the effects of urea on the wet strength of corn flour, soy flour and soy isolates. Additionally, the study aimed to relate these effects to the structural changes induced by urea and aimed to understand how the specific properties of these proteins contribute to the overall adhesive performance. The goal was to enhance the attractiveness of protein adhesives for industrial applications. Methods used included intrinsic fluorescence of tryptophan, tensile shear strength testing using an Automated Bonding Evaluation System (ABES), complex viscosity measurements, dynamic light scattering (DLS) and multi-angle light scattering (MALS). We were able to disprove the widespread assumption that urea as a denaturant improves the strength of protein adhesives due to a more elongated form of the protein and a higher availability of functional groups. Our results indicated that a spherical shape is more plausible than a cylindrical one, even in the presence of urea. Urea primarily caused a higher particle diameter, possibly due to aggregation. Moreover, wet strength values decreased when urea was added to soy flour and soy isolate. A different trend for was observed for corn flour. However, it seemed more likely that its higher hydrophobic content of amino acids and possibly its larger particle size contributed to higher wet and dry strength in samples with low moisture content. Corn flour, which is readily available worldwide, is therefore a good alternative to soy flour, which is not available in large quantities in Europe. Both are less expensive compared to protein isolates, but still need to be modified to meet the requirements of commercial products.

Key words: corn flour, soy flour, soy isolate, urea, intrinsic fluorescence of tryptophan, ABES, DLS, MALS, particle size, wet strength

Kurzfassung

Nachhaltige Proteinklebstoffe können aufgrund ihrer begrenzten Nassfestigkeit und höheren Produktionskosten nur schwer mit erdölbasierten Klebstoffen konkurrieren. In dieser Studie untersuchten wir die Auswirkungen von Harnstoff auf die Nassfestigkeit von Maismehl, Sojamehl und Sojaisolaten. Darüber hinaus sollten diese Effekte mit den strukturellen Veränderungen in Verbindung gebracht werden, die durch Harnstoff hervorgerufen werden, und es sollte geklärt werden, wie die spezifischen Eigenschaften dieser Proteine zur gesamten Klebstoffperformance beitragen. Das Ziel bestand darin, die Attraktivität von Proteinklebstoffen für industrielle Anwendungen zu erhöhen. Zu den angewandten Methoden gehörten die intrinsische Fluoreszenz von Tryptophan, die Prüfung der Zugscherfestigkeit mit einem "Automated Bonding Evaluation System“ (ABES), komplexe Viskositätsmessungen, dynamische Lichtstreuung (DLS) und Mehrwinkel-Lichtstreuung (MALS). Wir konnten die weit verbreitete Annahme widerlegen, dass Harnstoff als Denaturierungsmittel die Festigkeit von Proteinklebstoffen durch eine länglichere Form des Proteins und eine höhere Verfügbarkeit von funktionellen Gruppen verbessert. Unsere Ergebnisse deuteten darauf hin, dass eine kugelförmige Form für alle Proteine plausibler ist als eine zylindrische, selbst in Gegenwart von Harnstoff. In erster Linie verursachte Harnstoff einen höheren Partikeldurchmesser, möglicherweise aufgrund von Aggregation. Außerdem sanken die Werte für die Nassfestigkeit, wenn Sojamehl und Sojaisolat Harnstoff zugesetzt wurde. Ein anderer Trend wurde bei Maismehl beobachtet. Es schien jedoch wahrscheinlicher, dass der höhere hydrophobe Anteil von Aminosäuren und möglicherweise die größere Partikelgröße zu höheren Nass- und Trockenfestigkeit in Proben mit niedrigem Feuchtigkeitsgehalt beitrugen. Maismehl, das weltweit leicht erhältlich ist, ist daher eine gute Alternative zu Sojamehl, das in Europa nicht in großen Mengen verfügbar ist und importiert werden muss. Beide sind im Vergleich zu Proteinisolaten kostengünstiger, müssen aber noch modifiziert werden, um den Anforderungen kommerzieller Produkte zu entsprechen.

Schlüsselwörter: Maismehl, Sojamehl, Sojaisolat, Harnstoff, intrinsische Fluoreszenz von Tryptophan, ABES, DLS, MALS, Partikelgröße, Nassfestigkeit

1. Introduction

In recent years growing environmental awareness has encouraged the replacement of non-renewable resources like concrete and fossil fuels with wood and wood-based products. However, an environmentally friendly life cycle for wooden items and the production of a fully sustainable product requires the use of a sustainable adhesive. Unlike fossil-based adhesives, which are commonly used nowadays, sustainable adhesives such as lignin-, starch-, or protein-based ones are promising alternatives. These eco-friendly options, as highlighted by Dunky (2021), could replace non-sustainable materials like urea- or phenol-formaldehyde adhesives, contributing to the overall sustainability of wooden products (Dunky, 2021; Niemz et al., 2023).

In particular, protein-based adhesives have long been produced from a variety of protein sources, including animal protein, casein from milk, soy flour, and blood (Pizzi & Mittal, 2003). In the 1960s, synthetic adhesives eventually replaced protein-based adhesives in most applications due to their increased durability, greater cost effectiveness, and increased production efficiency. Proteins, particularly those found in soybean flour, have only experienced a slight resurgence as a significant adhesive for non-structural interior wood products in recent decades (Frihart et al., 2013). Various plants could be used as a resource to produce protein adhesives. However, to reduce emissions, achieve a better cost structure through short transport distances, and be more independent from global markets, it is desirable to use proteins that are produced in close proximity to where they are used. For reasons of cost efficiency, protein should also be a by-product of another production process and not intended for human consumption.

With a protein content of 36 %, soybeans have the highest protein level of all plant-based raw materials, making them one of the most widely used industrial protein sources (Dunky, 2021). In addition, as a by-product of oil production soy flour is inexpensive and easy to process. It is grown in large quantities in Brazil, the USA, Argentina, China and India (**Fehler! Verweisquelle konnte nicht gefunden werden.**), while the use of soy flour products for human food consumption is small (Vnučec et al., 2017). In Europe, proteins from wheat, potatoes and corn, among others, can be used for this purpose (Averina et al., 2021; Averina et al., 2023). In addition, corn is widely available in the USA, China, Brazil, the European Union and Argentina (**Fehler! Verweisquelle konnte nicht gefunden werden.**). Furthermore, it is particularly interesting, as it is available in large quantities as a by-product obtained from starch production, even if corn has a lower protein content of 10 % (Lásztity, 1996).

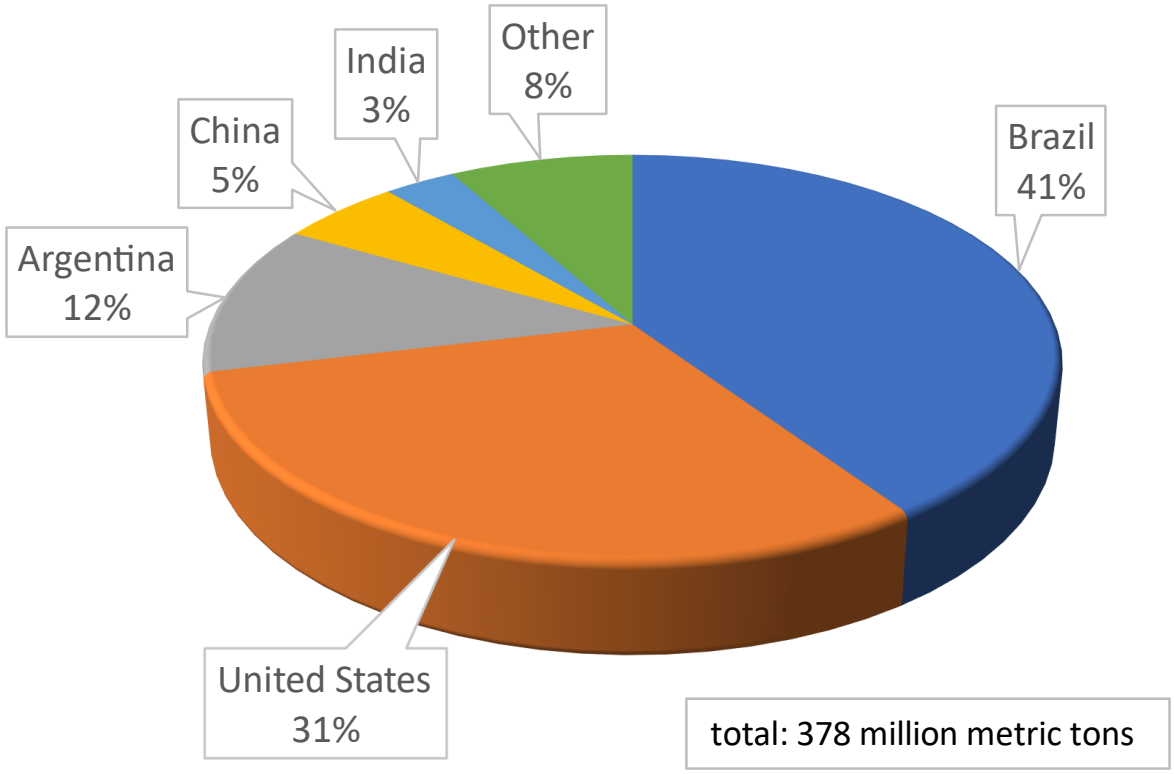

Figure 2: Soybean producing countries 2022/2023 (STATISTA, 2023)

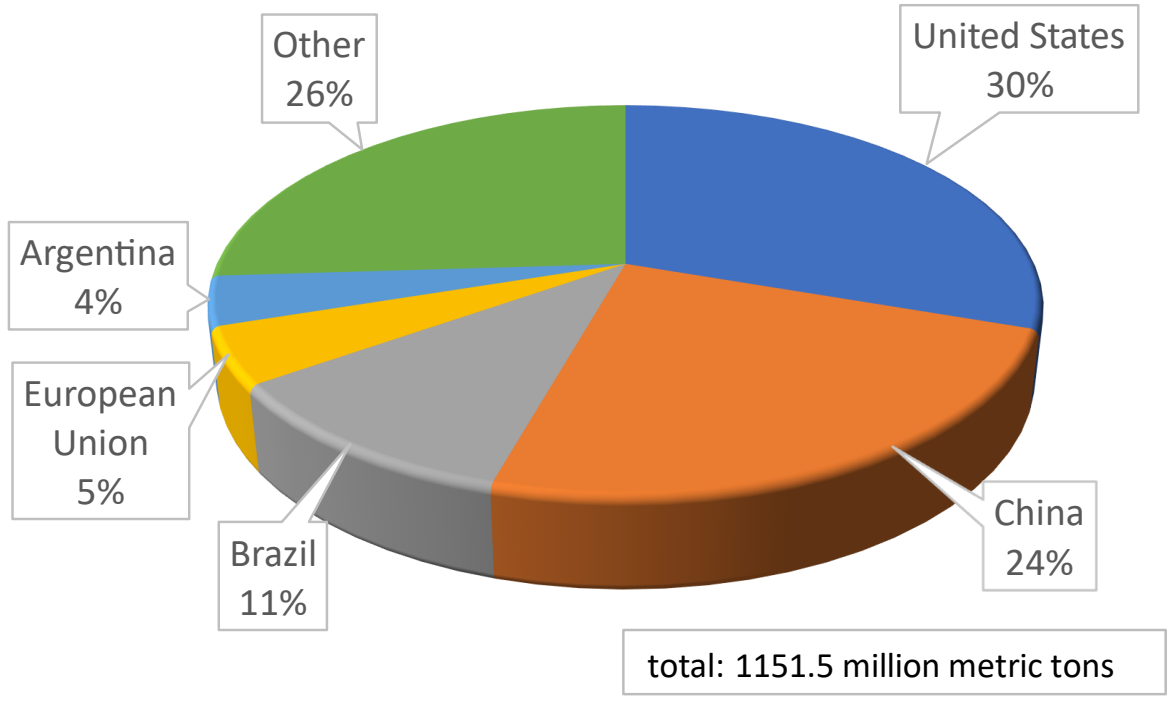

Figure 1: Corn producing countries 2022/2023 (STATISTA, 2023)

In general, proteins are expected to experience hydrophobic collapse in water at room temperature, and therefore be hard, have minimal surface area for interactions with neighboring proteins, and have limited capacity to coalesce into a strong film. A more open, flexible protein structure afforded by high urea concentration could theoretically result in more inter-protein interactions, more molecular entanglement between neighboring proteins, and better film coalescence because the urea-exposed proteins would presumably be more flexible. Inter-protein interactions, polymer entanglement, and better film coalescence would all presumably be causing an increase in strength.

Most protein adhesives already show good dry strength and high wood failure in adhesive tests (Dunky, 2021; Kallakas et al., 2024). In North America, more than half of interior plywood is produced with soy protein-based adhesives (Hunt et al., 2022). Similar commercial options are lacking in Europe. Insufficient wet strength of all protein adhesives limits an expanded use in European interior plywood and in other, higher volume markets such as particleboard or fiberboard (FAO, 2019). To address this issue, techniques like crosslinking and chemical or physical modifications are necessary to enhance cohesion and promote coalescence. Based on Dunky (2021), changing the native structure of proteins plays a key role in exposing functional groups within them and facilitating bonding via hydrogen bonds. Native proteins typically adopt highly folded structures, where hydrophobic groups are largely shielded from contact with substrates. Therefore, denaturation is a crucial step to expose these groups according to Dunky (2021), Y. Zhang et al. (2018) and B. Zhang et al. (2022). Denaturation can be achieved through various methods such as thermal treatment, exposure to acids or alkalis, organic solvents, enzymes and detergents, such as urea (Damodaran, 2017; Dunky, 2021). Huang and Sun (2000) claimed that the addition of urea to soy protein adhesives increased dry strength, although they did not test soy with 0 M urea and did not conduct wet tests. (Z. Zhang & Hua, 2007)Z. Zhang and Hua (2007) performed the appropriate controls and found that 1 M urea is ideal for dry bonding with glycinin soy protein but has little effect on ß-conglycinin protein. On the contrary, Kallakas et al. (2024) identified a direct correlation between the surface hydrophobicity and the wet strength of soy protein adhesives.

Due to differing opinions in the literature as to which protein properties increase wet strength, our main objective in this study was to identify possible structural changes in corn flour, soybean flour and soy isolate caused by urea and correlate these effects to the wet strength of protein adhesives. In particular, we wanted to test the hypothesis if proteins in the presence of denaturants such as urea adopt an elongated form, so that more functional groups are available to interact with neighboring proteins. Therefore, we wanted to find out whether the presence of urea improves the accessibility of the amino acid tryptophan to the solvent, or otherwise influences the size and/or structure of the protein particles.

2. Theoretical background

2.1. Intrinsic fluorescence spectroscopy

Fluorescence is defined by the interaction of light and matter at the atomic or molecular level. A fluorescent molecule absorbs photons, usually from ultraviolet or visible light sources, and then emits photons at longer wavelengths within nano seconds. Fluorescence is caused by the transition of electrons within atoms or molecules from a ground state to an excited state when light is absorbed. Following that, the excited electrons return to their ground state and emit excess energy in the form of fluorescent light. This emission is always longer in wavelength than the absorbed light, resulting in a distinct spectral shift. This phenomenon is defined by complex quantum mechanical principles and is influenced by variables such as molecular structure, environment, and interactions with neighboring molecules (Atkins & Paula, 2006).

Intrinsic fluorescence spectroscopy is often used to study the structure and behavior of proteins, as proteins contain three amino acids (tryptophan, tyrosine, and phenylalanine) that are naturally fluorescent due to their aromatic rings (Atkins & Paula, 2006). Considering that phenylalanine has a very low quantum yield and emission by tyrosine in native proteins is often quenched, tryptophan has the highest intrinsic fluorescence (Akbar et al., 2016). In terms of its structure, tryptophan contains a large indole ring, which absorbs strongly in the near-ultraviolet wavelength of the spectrum, with a maximum excitation wavelength around 280 nm. Following excitation, tryptophan emits fluorescent light with a wavelength dependent on the hydrophobicity of its environment (Atkins & Paula, 2006).

When studying protein fluorescence, the quenching process reveals fascinating insights into the complex nature of protein emission spectra. In particular, researchers have observed a consistent shift to lower wavelengths during the quenching process, indicating the presence of multiple components in these spectra (Reshetnyak & Burstein, 2001). To disentangle these different spectra, deconvolution is a widely used method that provides a systematic approach to isolate individual components. In particular, deconvolution plays a central role in the analysis of tryptophan fluorescence emission spectra, where a lognormal fit is often used for precise delineation (E. Burstein & Emelyanenko, 1996). These spectra, whose maximum peak lies between 308 (most hydrophobic environment) and 353 nm (most hydrophilic environment), are divided into five different classes, each reflecting different tryptophan environments in proteins. By applying a deconvolution, this method effectively quantifies the contributions of these environments to the overall fluorescence signal (Reshetnyak & Burstein, 2001).

Understanding the variability of the maximum position of tryptophan fluorescence, emphasizes the importance of the specific protein environment (Reshetnyak & Burstein, 2001). In addition, the position of the peak in the fluorescence emission spectrum serves as a crucial indicator for the accessibility of tryptophan. A red shift of the emission spectrum indicates that the indole ring of tryptophan is in a more hydrophilic environment, which could indicate the presence of more hydrophilic residues. Conversely, a blue shift may indicate that tryptophan is obscured or shielded by the solvent environment (Reshetnyak & Burstein, 2001; Sze et al., 2007).

Fluorescence quenching, which is characterized by a decrease in fluorescence intensity due to interactions with quenchers, is a widely studied phenomenon in molecular spectroscopy. The Stern-Volmer equation (Equation 1) serves as a basic tool for analyzing quenching dynamics and relates fluorescence intensity in the presence (F) and absence (F_0) of a quencher. Plotting F_0/F against quencher concentration provides insight into quenching kinetics and molecular interactions (Lehrer, 1971). A steeper slope in the Stern-Volmer diagram indicates greater accessibility of tryptophan to the quencher. However, it is important to note that the Lehrer equation provides primarily qualitative information, as it assumes the presence of two different types of tryptophan: quencher accessible and inaccessible to tryptophan. However, research by E. A. Burstein et al. (1973) and Reshetnyak et al. (2001) challenges this assumption and points to the variability in the accessibility of tryptophan in different proteins. To obtain a more accurate quantitative analysis, fluorescence quenching data are often subjected to deconvolution, as previously described.

$$\frac{F_0}{F} = 1 + K_{SV}[Q] \qquad \text{(Equ. 1)}$$

2.2. Light scattering

Light scattering is a phenomenon that occurs when electromagnetic radiation, such as light, interacts with particles suspended in a medium. This interaction arises from the oscillating electric fields associated with both the incident light and the particles themselves. As the incident light encounters these particles, its electric field induces dipole moments in the particles, resulting in the scattering of light in various directions (Atkins & Paula, 2006).

DLS determines the hydrodynamic diameter of particles suspended in a liquid medium by analyzing fluctuations in scattered light intensity over time. It relies on the principle of Brownian motion. This motion occurs due to the random collisions of particles with solvent molecules,

as described by the Stokes-Einstein relationship, which correlates particle diffusion coefficients with their hydrodynamic size. Furthermore, the scattering of light by particles depends on their size in relation to the wavelength of the incident light (Stetefeld et al., 2016).

The standard scattering angle for DLS measurements is 90°. For particles with less than 50 nm hydrodynamic diameter, the best signal to noise and measurement reproducibility can be achieved by using the backscattering angle of 173° (Brookhaven Instruments, 2024) because if many small particles are present in the sample, this can lead to multiple scattering of light, i.e. the scattering of a photon by more than one particle as opposed to the scattering of a photon by just one particle. When measuring in backscatter mode, light does not pass through the entire sample in the cuvette, which facilitates the measurement of smaller particle sizes and highly concentrated samples. In general, larger particles rather tend to scatter the light in the forward direction, so that when measuring in backscattering mode, their contribution to scattering is avoided due to the different measuring angle (Stetefeld et al., 2016).

Intensity-based data is the most reliable and reproducible one for DLS data. Since larger particles scatter more light than smaller ones, this should be considered when interpreting data, as few large particles might have the same or a higher contribution than many small particles (Malvern Instruments Limited, 2017). To find out more details about the measured samples, one can analyze volume-based data as well. To do that, a repeatable correlation function is important. Furthermore, it should be considered that a spherical shape is used as the basis for all calculations, although the real shape may differ, when analyzing volume-based data obtained from a DLS device (Nobbmann, 2017).

In contrast to DLS, which focuses on particle size based on scattered light fluctuations, MALS measures the angular dependence of scattered light intensity at multiple angles. This provides valuable information about particle size, shape and molecular weight and is therefore particularly useful for the comprehensive characterization of particles (Wyatt, 1997).

3. Materials and Methods

3.1. Materials

Three different proteins were used for this study, two protein-containing flours and one protein isolate. Corn gluten flour, abbreviated as CornF in this investigation, was provided by AGRANA Stärke GmbH (Aschbach, Austria) and was a dried by-product of starch extraction from corn. According to AGRANA Stärke GmbH, it consisted of about 60 % protein. Soy flour Prolia™ 100/90, hereinafter referred to as SoyF, was purchased from Cargill (Minneapolis, MN, USA). It was a by-product of oil extraction of soybeans and contained between 50 and 55 % protein (Liu, 1997). This soy flour was sieved with a USA mesh size of 100, which corresponded to 0.149 mm, and had a protein dispersibility index of 90. The protein dispersibility index compares the solubility of a protein in water from 0 – 100 %, with 90 % being a very good solubility (AOCS, 2017a). The third protein used was a self-produced soy protein isolate in its native state, abbreviated as NSPI in this research paper. It was produced by the Forest Products Laboratory in February 2023. It contained between 90 and 95 % protein (Liu, 1997) and exhibited native properties in differential scanning calorimetry measurements. The production process can be found in Hunt et al. (2022), where the term PPSPI was used for the soy protein isolate.

Potassium iodide was purchased from Mallinckrodt (Dublin, Ireland). Phosphoric acid, potassium hydroxide, urea, L-Tryptophan (hereinafter referred to as Try), 1.5 M hydrochloric acid, and 1.5 M sodium hydroxide were purchased from Sigma-Aldrich (Milwaukee, WI, USA).

Considering that a different pH is causing a peak shift in fluorescence spectra (Gandhi, 2002), two buffer solutions were used for all subsequent tests. One was a 0.1 M phosphate buffer, subsequently denoted as "P-buffer", and the other was a 0.1 M phosphate buffer mixed with 6 M urea, hereafter referred to as "U-buffer". The pH of both was adjusted to 7.2 and both solutions were filtered with a Type HA 0.45 µm filter from MilliporeSigma (Burlington, MA, USA). When protein concentrations of 15 wt. % or 30 wt. % were used, the buffer capacity was not sufficient to set a pH of 7.2. Therefore, the pH for these samples was adjusted manually.

In addition, soy flour generally contains the enzyme urease, which increases the pH in the presence of urea by forming carbon dioxide and ammonia (AOCS, 2017b). To counteract this when using our U-buffer, a batch of SoyF was pre-treated. It was mixed with deionized water and the pH was then lowered to 4.5 with 1.5 M HCl to destroy the ureases. The viscous slurry was spread on aluminum foil and dried in an oven at 60 °C. The pre-treated SoyF was used in all experiments with SoyF and U-buffer.

3.2. Conducted experiments - overview

To provide a comprehensive overview of the conducted experiments,

Figure 3 presents a summary. All experiments utilized both P-buffer and U-buffer to investigate the impact of urea on protein structure and adhesive strength. Relatively low and high concentrations were selected to be able to use specific methodologies and to analyze the influence of concentration in fluorescence emission spectra. Furthermore, fluorescence emission spectra and KI quenching were performed on the supernatant of NSPI, because native soy protein isolates should be completely soluble when in the native state. After centrifugation however, a pellet was detected on the self-produced NSPI, which was not used for the respective experiments.

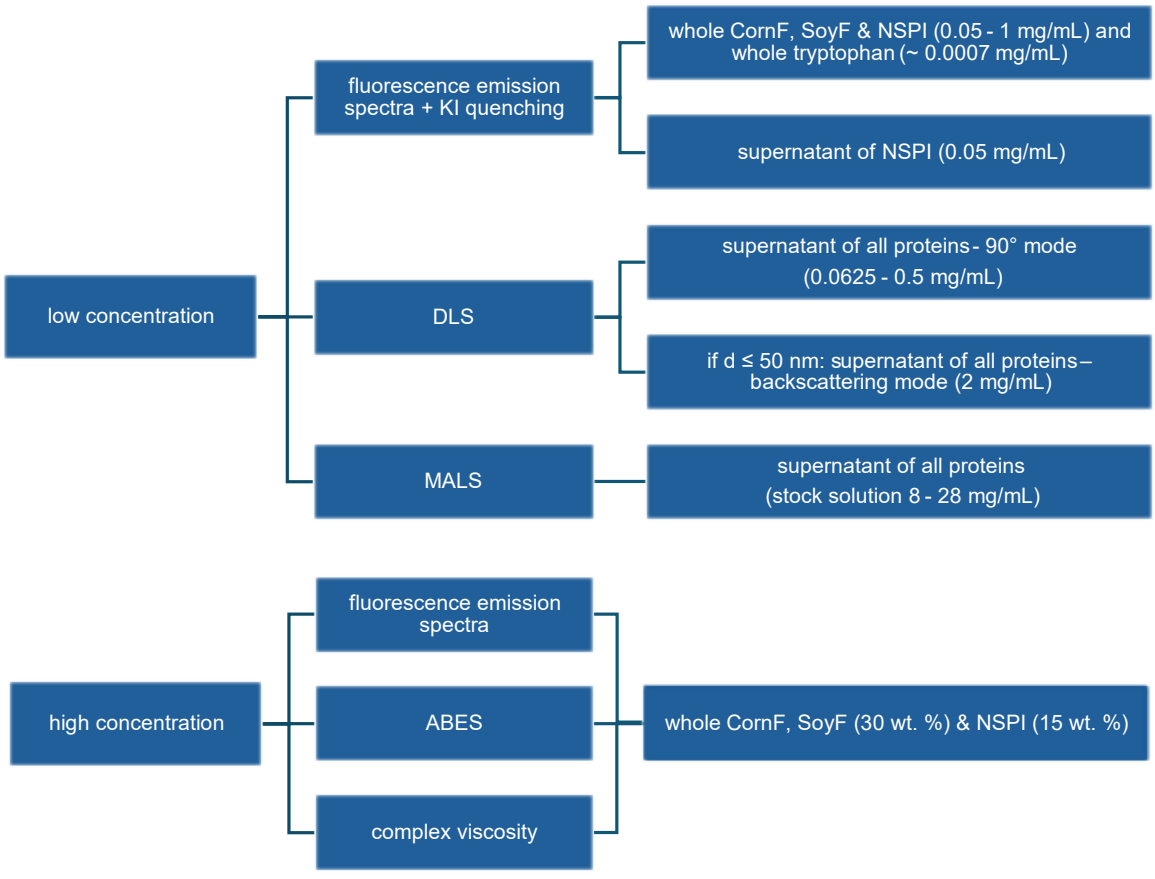

Figure 3: Conducted experiments with P-buffer and U-buffer with the final protein concentrations.

3.3. Intrinsic fluorescence emission spectra

A stock solution of 5 mg/mL for each protein (CornF, SoyF and NSPI) or 0.1 mg/mL for the amino acid Tryptophan with P-buffer or U-buffer was prepared for whole-low-concentration mixtures and agitated for one hour. For measurements of the NSPI supernatant in P-buffer and U-buffer stock solutions of 2 mg/mL were agitated for one hour and centrifuged (Avanti JXN-26 from Beckman Coulter, Inc. in Brea, CA, USA) at 6870 G for 15 minutes at 23 °C. Following centrifugation, the concentration was determined using a UV-Vis spectrometer (UV-1900 i from Shimadzu Corporation in Kyoto, Japan). Stock solutions of whole and centrifuged samples were then diluted accordingly to reach the top limit of our fluorescence spectrometer's linear range. While measuring whole-low-protein-concentrations, samples were stirred in the cuvette using a magnetic stirrer to ensure a homogenous particle distribution. To quench low-concentration samples, a 5 M potassium iodide (KI) stock solution was freshly prepared each day due to its low stability and increased absorbance with time. Appropriate aliquots of this KI stock solution were then mixed with an initial protein-solution-volume of 3 mL to reach the final concentration displayed in the figures. For measurements with high-protein-concentrations, 30 wt. % solids content for protein flours and 15 wt. % solids content for protein isolate were stirred with P-buffer or U-buffer. All samples were agitated for 30 minutes at 600 rpm using a high shear mixer (Hei-TORQUE 400 from Heidolph Instruments GmbH&CO.KG in Wood Dale, IL, USA). Fluorescence emission spectra and fluorescence quenching data for low-protein-concentrations and fluorescence emission spectral data (Fluorolog Tau-2 from JY-Horiba in Edison, NJ, USA) for high-concentrations were obtained using a quartz cuvette (Starna Cells, Inc. in Atascadero CA, USA).

For all measurements an excitation wavelength of 280 nm and an emission spectrum of 300 to 400 nm was selected. Our fluorescence spectrometer has double grating for both excitation and emission, so a total of four calipers limit the slit width (or bandwidth) of light. The first two calipers between the xenon arc lamp and the sample were each set to 8 mm, which corresponds to a bandwidth of 15.7 nm, so that as many photons as possible reach the sample. The other two calipers between the sample and the photomultiplier tube were set to 5 mm (8.6 nm) and 1.5 mm (3.7 nm) to achieve a narrow resolution. In addition, we used a 1.5 OD neutral-density filter or switched between a right-angle and front-face measuring mode to adjust the number of measured photons. An integration time of three seconds was selected for all low-concentration measurements with visible particles. Otherwise, one second for the supernatant and high-concentration samples was used.

In general, four spectra, two each from two separate mixtures, were averaged and used for analysis. For data processing Python 3.10 was used. Fluorescence spectra were fitted with a

lognormal fit and normalized data were deconvoluted into three peaks. Normalization was carried out to enable a direct comparison on the one hand and to be more robust against fluctuations in the original intensity on the other. The center of the three peaks used for the deconvolution analysis was selected at 308, 331 and 353 nm with a fluctuation range of 4 nm each.

3.4. Adhesive bonding tests

Adhesive bonding tests according to ASTM International (2019) were performed with an ABES device (Model 311c from Adhesive Evaluations Systems, Inc. in Corvallis, OR, USA) (Figure 4). The same highly concentrated protein mixtures used for previously described fluorescence measurements and sugar maple *(Acer saccharum)* veneer strips from Columbia Forest Products (Greensboro, NC, USA) were used. Veneers were stored at controlled temperature (21 °C) and relative humidity (50 %) prior to cutting. They had a thickness of 0.7 mm and were cut into 117 x 20 mm strips with a pneumatically driven sample cutting device for standardized ABES samples preparation (Adhesive Evaluations Systems, Inc. in Corvallis, OR, USA). Adhesive was spread on an overlapping area of 20 x 5 mm between two veneers and all samples were pressed at 150 °C for 120 seconds with a pressure of 1.5 N/mm^2. Afterwards the samples were stored in three different conditions (Figure 5) before they were tested for tensile shear strength. For each adhesive mixture, 6 samples per set were tested, making a total of 18 samples per adhesive mixture.

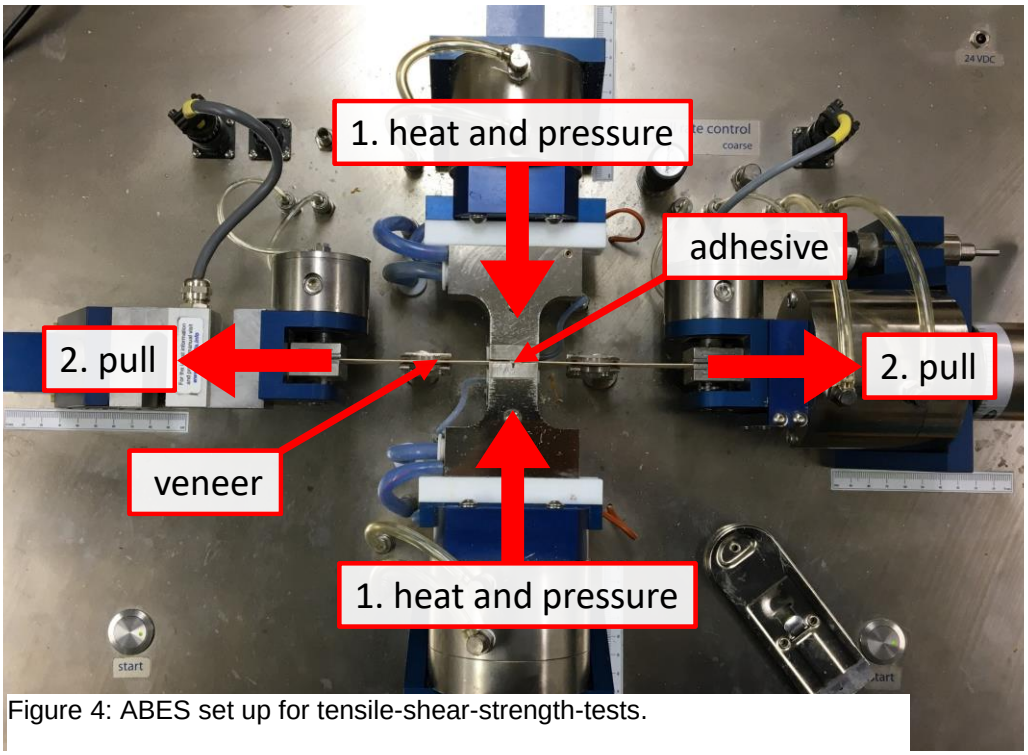

Figure 4: ABES set up for tensile-shear-strength-tests.

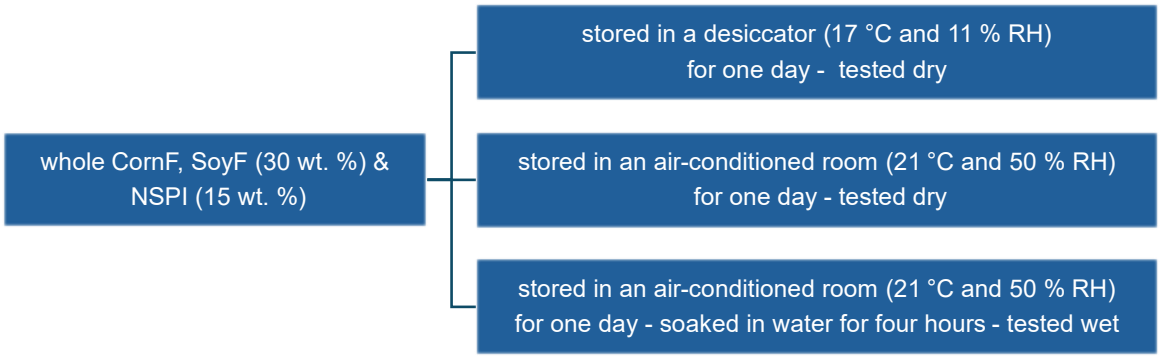

Figure 5: Storing and testing conditions of high-protein-concentration samples for tensile-shear-strength-tests.

3.5. Complex viscosity

Additionally, complex viscosity of the same highly concentrated protein mixtures was measured using a rheometer (Anton Paar MCR302 in Graz, Austria) equipped with a cup and bob. A concentric cylinder with a diameter of 27 mm and a cylindrical Peltier thermal device (C-PTD200) were used. Approximately 20 g of sample were filled into the cup. After introducing the measurement tool, sample temperature was allowed to stabilize at 26.7 °C for five minutes. To minimize surface evaporation Parafilm M® strips were applied onto the cup's surface, extending coverage as much as possible without touching the stem of the measuring body. The rheological measurement itself consisted of a 25-point oscillatory amplitude sweep, increasing the shear strain gradually from 0.01 % to 1000 % logarithmically at a constant frequency of 1 Hz. Two measurements per mixture were performed.

3.6. Particle characterization via light scattering

3.6.1. DLS

A NanoBrook Omni (Brookhaven Instruments in New York, USA) instrument was used to determine the hydrodynamic diameter of the soluble portion of our proteins in our two different solutions. Protein solutions between 2 and 50 mg/mL were first agitated for one hour when measured in 90°-measurement-mode and four hours when measured in backscattering-mode to increase the dissolved protein content in the solution. After mixing, samples were centrifuged at 6870 G for 15 minutes at 23 °C. The concentration after centrifugation was

determined and adjusted to a suitable concentration between 2 and 0.0625 mg/mL, as a higher concentration is required for smaller particles. Samples were stored in a refrigerator at 5 °C for one day prior to measurement to achieve a better correlation, especially with larger particles. After inserting the cuvette into the device, an equilibration time of five minutes was selected. The laser's wavelength was 659 nm. Five measurements of the same sample were made with the instrument set to 25 °C and a measurement time of 180 seconds. Additionally, a 40 nm dust cut-off limit was selected. If the effective diameter was around 50 nm for measurements with the 90°-measuring-mode, replicates were also tested in backscattering-modus. A total of four measurements per combination, two each from two separate mixtures, were averaged.

3.6.2. MALS

To determine the shape of the soluble part of our proteins, MALS measurements were conducted. For this, protein and P-buffer or U-buffer were mixed at a concentration of 20 - 50 mg/mL for four hours and then centrifuged at 6870 G for 15 minutes at 23 °C. After centrifugation, the concentration was determined using a UV-Vis spectrometer. For all measurements an integration time of 80 sec was selected. 30 mL of the corresponding buffer was filled into a 40 mL vial and measured as a reference. Subsequently, 1 mL of the centrifuged protein solution was continuously added to the vial and a five-minute equilibration time was observed before a new measurement was performed. This was repeated until the results no longer showed 0 for at least three runs. One measurement was carried out for each combination.

These measurements were performed using a house-built device (Figure 6). The device had five lasers with wavelengths of 800, 636, 527, 451 and 405 nm and five detectors arranged in a semicircle around the sample holder to detect scattered light from different angles, which were 160°, 128°, 96°, 64° and 32° in relation to the incident beam. Data acquisition and initial analysis was performed using a code written in Python. Here, the refractive index was assumed to be 1.33 for the P-buffer and 1.38 for the U-buffer (Warren & Gordon, 1966). The refractive index increment, which is the change in refractive index per unit concentration of solution, was set at 0.18 (Barer et al., 1953).

To determine the shape of scattering particles, SasView 5.0.6 was used to analyze our MALS data with two different methods. For an objective analysis without assuming a specific particle shape, MALS data were fitted with a Guinier model and radius of gyration ($R_{g\ Guinier}$), which corresponds to the effective size of the scattering particles, was determined. $R_{g\ Guinier}$ was then divided by the hydrodynamic radius (R_h) of the DLS measurements. Based on the

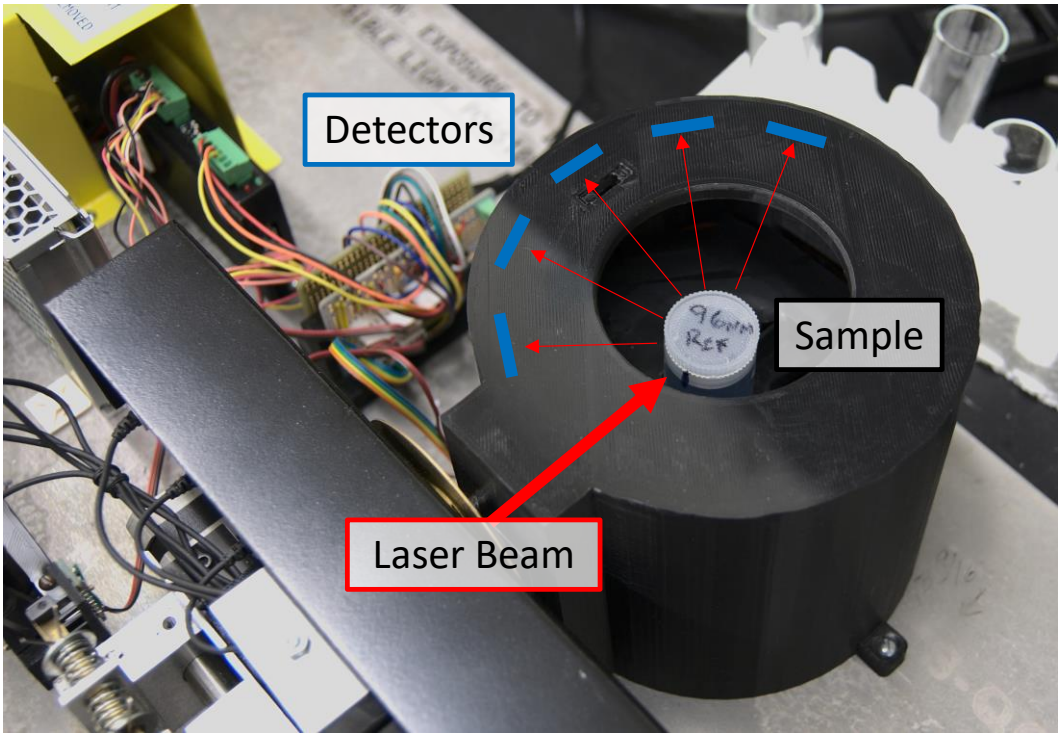

Figure 6: MALS device with 5 different lasers and detectors (picture from Carl Houtman).

ratio, assumptions about the shape can be made (Table 1) (Glatter, 1983). Subsequently, our preliminary MALS data were fitted using a polydisperse sphere model and a polydisperse cylinder model. For P-buffer 1.33 was chosen as scattering length density and 1.38 for U-buffer. Scattering length density of proteins was set at 1.4 and a polydispersity of 1 was assumed. The equivalent $R_{g\,Sph}$ and $R_{g\,Cyl}$ for these shapes were calculated using Equations 2 and 3 (Glatter, 1983). These results were again divided by R_h to analyze the value of the ratio. The values of the sphere and cylinder models were then compared with $R_{g\ Guinier}$ to determine which model was more plausible.

Table 1: Shape assumption of particles based on the ratio of R_g / R_h.

R_g / R_h	**Shape**
1.6	extended rod
1.3	random coil structure
0.8	solid sphere

$$R_{g\,Sph} = \sqrt{\frac{3}{5} \cdot R_{Sph}^2} \qquad \text{(Equ. 2)}$$

$$R_{g\,cyl} = \sqrt{\frac{L^2}{12} + \frac{R_{Cyl}^2}{2}} \qquad \text{(Equ. 3)}$$

3.7. Statistical Analysis.

The statistical analysis involved utilizing Python 3.10 to conduct a Kruskal-Wallis test and a Dunn post hoc test to determine the significance of observed data patterns. The Kruskal-Wallis test checked for significant differences between three or more groups. This test was chosen due to the non-normal distribution of the data and the lack of homogeneity in variances. As a post hoc test a Dunn test was performed to determine which groups differed significantly from each other. The significance level was set at 0.05, indicating that results were considered meaningful if the probability of them occurring by random chance was less than 5 %.

4. Results

4.1. Intrinsic fluorescence emission spectra

Three illustrative results of the lognormal deconvolution of normalized fluorescence emission spectra at 280 nm excitation into hydrophobic, mixed and hydrophilic fractions are shown in Figure 7. The upper plot shows that whole CornF in P-buffer at low concentration had larger hydrophobic and hydrophilic peaks with less spectral overlap. Whereas, SoyF and NSPI had a relative larger fraction of the mixed component and a peak at 333 nm. This

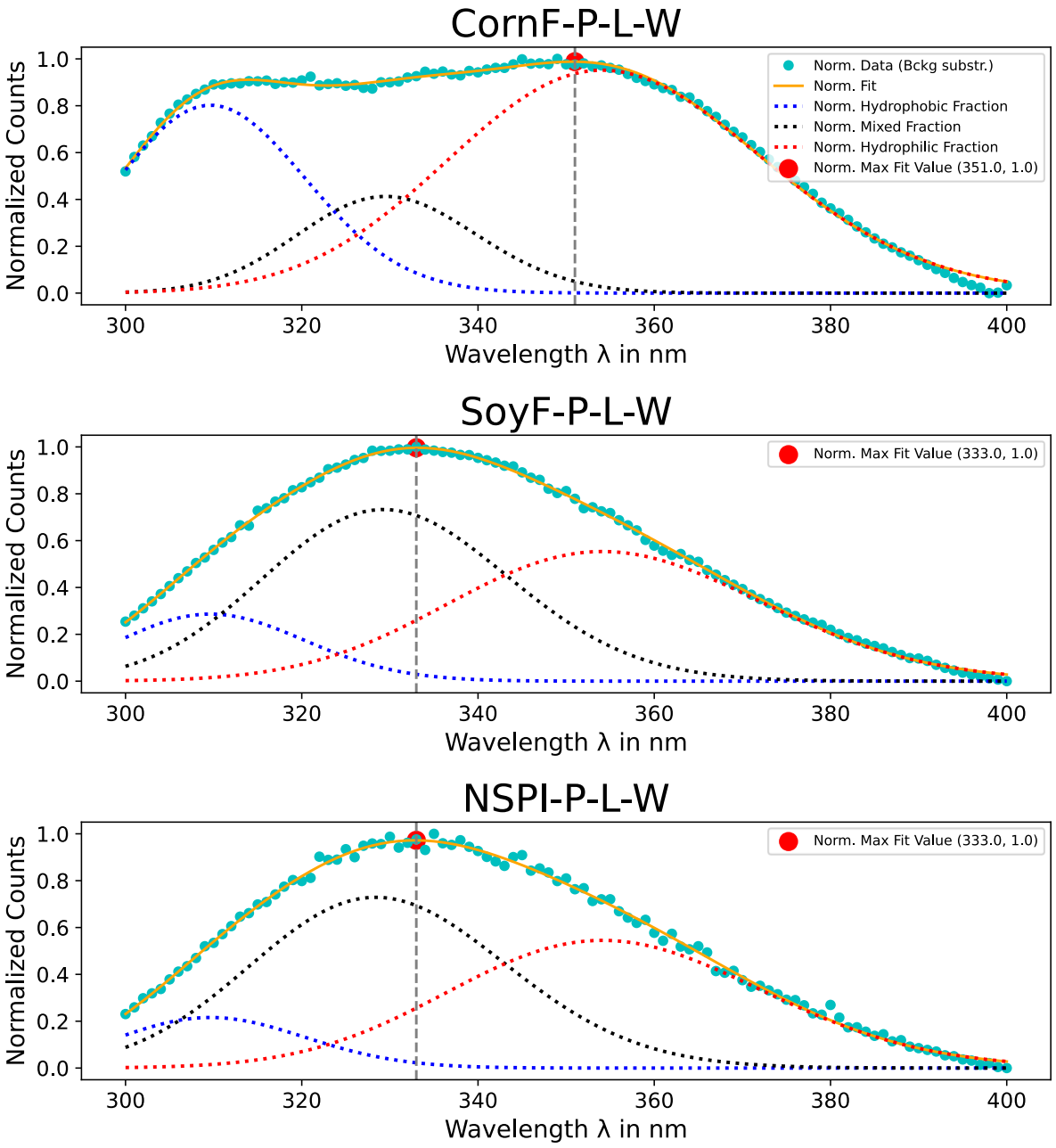

Figure 7: Fluorescence emission spectra for whole (W) CornF, SoyF and NSPI in P-buffer (P) at low concentrations (L).

distinction was consistently observed under different conditions, including different buffers (P-buffer and U-buffer), protein concentrations (30 wt. % or 15 wt. % and less than 1 mg/mL) and sample conditions (whole and supernatant), revealing a clear difference between corn and soybean in the fluorescence emission spectra.

Figure 8 depicts λ_{max} for all combinations, excluding CornF due to its bimodal peak presence. All proteins consistently demonstrated a red shift when urea was present in the buffer. Tryptophan in both P-buffer and U-buffer reached an approximate maximum peak at 353 nm, in accordance with existing literature (Reshetnyak & Burstein, 2001). Upon comparison with the proteins, minimal difference was noted between Tryptophan and SoyF-U-H, measuring 9.5 nm, whereas maximum difference occurred between Tryptophan and NSPI-P-L-S, reaching 20.5 nm. Moreover, the distinction between P-buffer and U-buffer in highly concentrated protein samples was less pronounced than in low concentrations ($\Delta \lambda_{max}$ of 6 nm for SoyF and 4.5 nm for NSPI at high concentrations, compared to a $\Delta \lambda_{max}$ of 9 nm for SoyF, 7.3 nm for whole NSPI and 10.5 nm for centrifuged NSPI at low concentrations). At the same time, higher concentrations displayed a peak at a marginally higher λ_{max} compared to low concentration samples. Using the supernatant of NSPI resulted in a slight increase in the difference between P-buffer and U-buffer compared to non-centrifuged NSPI. The Kruskal-Wallis test, detected significant differences in λ_{max} among protein mixtures (p-value = 3.08e-06). The post-hoc Dunn test revealed specific pairwise differences. Notably, Try-P-L-W and

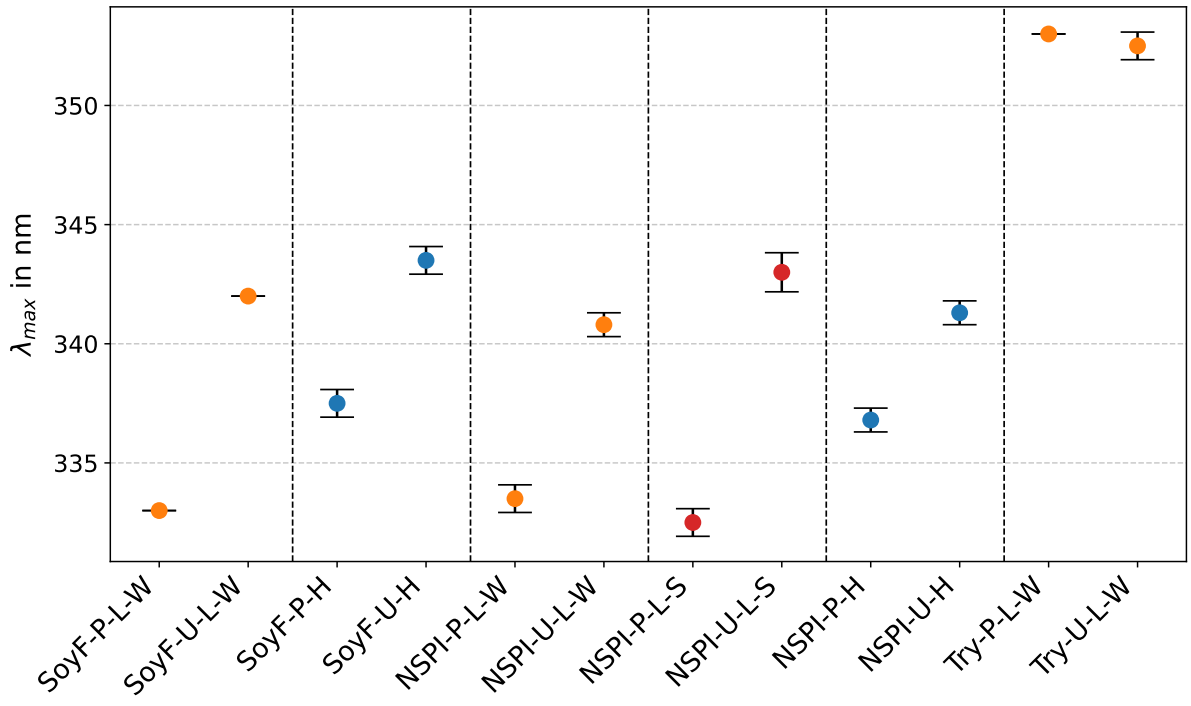

Figure 8: λ_{max} of SoyF, NSPI and Tryptophan in P-buffer (P) and U-buffer (U), at low concentrations (L) and high concentrations (H), whole protein (W) and supernatant (S).

Try-U-L-W exhibited the most pronounced significant distinctions in λ_{max} with SoyF-P-L-W, NSPI-P-L-W and NSPI-P-L-S. Furthermore, SoyF-U-H and NSPI-P-L-S were significantly different.

Fluorescence quenching of proteins and tryptophan by ionic solvents was performed on low concentration samples. During the quenching process, a spectral shift to lower wavelengths was observed, which supports the hypothesis that the emission spectrum of the proteins consisted of several components (Reshetnyak & Burstein, 2001). The findings are depicted in a Stern-Volmer plot (Figure 9). CornF was excluded from the analysis due to the presence of dual peaks in the fluorescence emission spectra. Interestingly, a consistent trend emerged, revealing a higher intensity drop in the presence of urea compared to just the buffer for all analyzed protein mixtures, which indicated better accessibility of Tryptophan. This trend was not observed with tryptophan, although the highest quenching rate was obtained. The initial intensity of Try-P-L-W could be quenched by nearly 5 times at an end concentration of 0.25 KI, while Try-U-L-W experienced a 4.77-fold drop at the same concentration. Proteins exhibited a less pronounced decrease in intensity. The most significant drop, 1.8 times, was observed for NSPI-U-L-S, whereas the smallest drop, 1.4 times, occurred with NSPI-P-L-W. At a concentration of 0.25 KI, the Kruskal-Wallis test indicated a statistically significant difference between the treatments ($p = 0.00012$). Significant pairwise differences between treatment groups were found using post-hoc Dunn's tests. A notable difference in KI

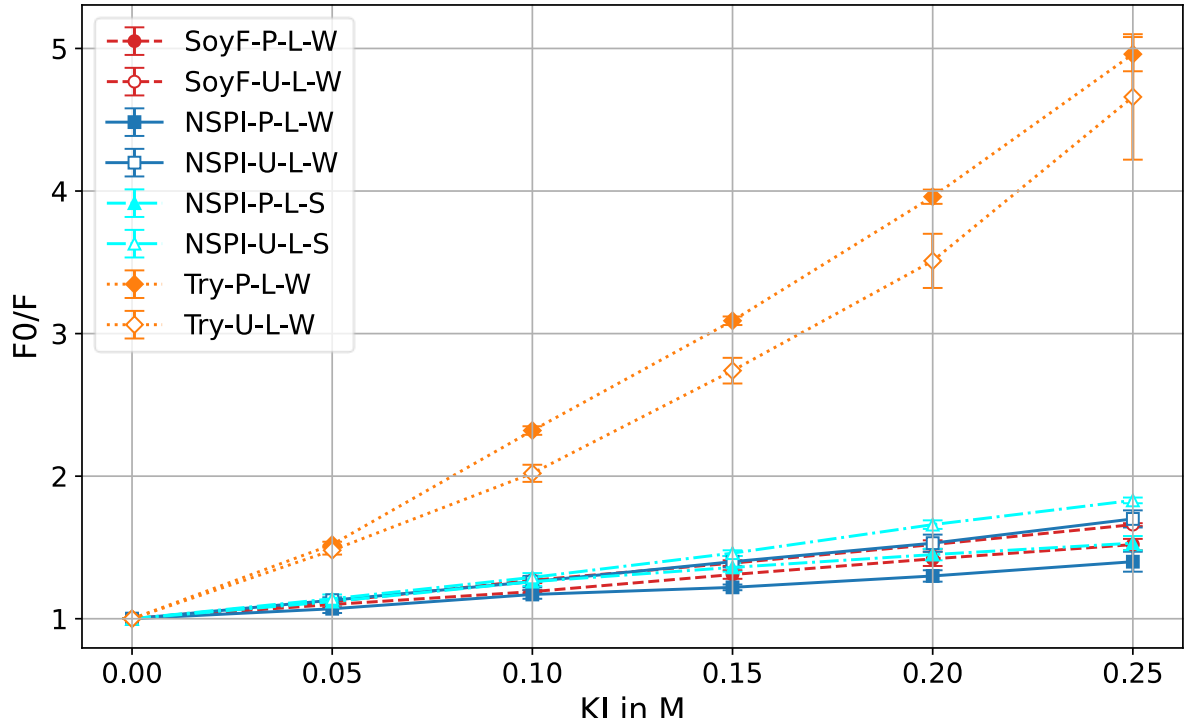

Figure 9: Quenching data in a Stern-Volmer plot of SoyF, NSPI and Tryptophan in P-buffer (P) and U-buffer (U), at low concentrations (L) and high concentrations (H), whole protein (W) and supernatant (S).

quenching responses was observed between SoyF-P-L-W and Try-P-L-W, NSPI-P-L-W and Try-P-L-W, NSPI-P-L-W and Try-U-L-W, and NSPI-P-L-S and Try-P-L-W. No significant difference between the other protein samples in P-buffer and U-buffer was found.

To illustrate the outcomes of deconvolution, Figure 10 presents a comprehensive summary of the normalized hydrophobic, mixed, and hydrophilic proportions in all protein combinations, including those subjected to KI quenching. Tryptophan in P-buffer and U-buffer generally showed the highest hydrophilic content of almost 100 %. Notably, CornF manifested the highest hydrophobic content in both P-buffer and U-buffer, and these ratios remained relatively constant in the presence of urea. While SoyF and NSPI displayed a lower hydrophobic ratio compared to CornF, all proteins exhibited comparable hydrophilic ratios in P-buffer at low concentrations. In SoyF and NSPI the introduction of urea tended to augment the hydrophilic fraction for low and high concentrations. At high concentrations SoyF in P-buffer and U-buffer, as well as NSPI in P-buffer, exhibit higher hydrophilic fractions than at lower concentrations, a trend which was not seen in NSPI in U-buffer. Minor distinctions were observed between whole NSPI and the supernatant of centrifuged NSPI.

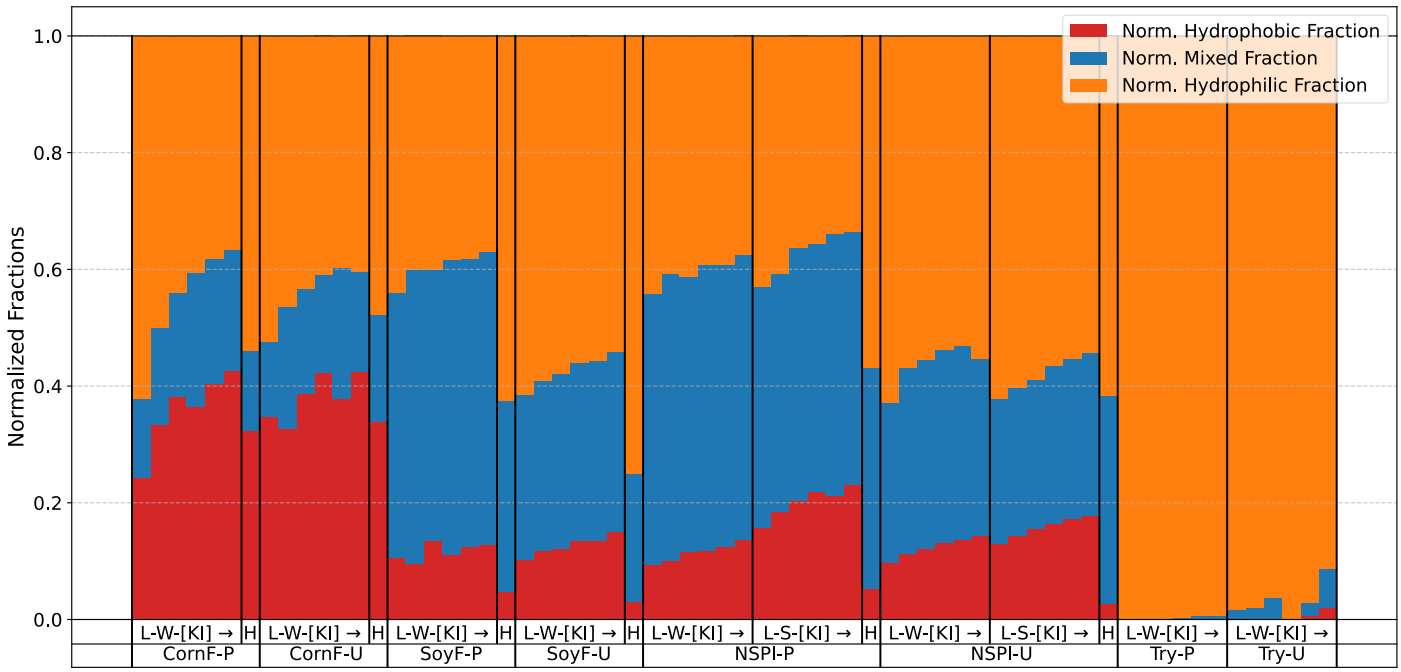

Figure 10: Hydrophobic, mixed and hydrophilic proportions of CornF, SoyF, NSPI and Try in P-buffer (P) and U-buffer (U), at low concentrations (L) and high concentrations (H), whole protein (W) and supernatant (S) with increasing KI concentration up to 0.25 M end concentration ([KI] →).

4.2. Adhesive bonding tests

Tensile shear strength was assessed for adhesive blends containing 30 wt. % solids content for CornF and SoyF and 15 wt. % solids content for NSPI (Figure 11). Each adhesive mixture in P-buffer and U-buffer underwent different storage conditions (compare Figure 5). Two different trends could be identified from these results. With CornF, tensile shear strengths either remained the same or increased when urea was present. For SoyF and NSPI, values either remained the same or decreased when the U-buffer was used. Looking at the values from the samples stored in the desiccator (17 °C and 11 % RH), CornF-U had the highest value at 8 N/mm^2, followed by Corn-P at 6.8 N/mm^2. SoyF and NSPI had lower values in this set, with NSPI-U having the lowest at 4.6 N/mm^2. This difference between CornF and SoyF/NPSI equalized slightly when the samples were stored at 50 % RH, indicating an indirect influence of sample moisture in CornF. SoyF had the lowest and NSPI the highest wet strength values. The higher amount of non-protein components appeared to have an indirect influence on wet strength in soy, with the difference between SoyF-P and NSPI-P being significant. However, the higher amount of non-protein components in CornF did not appear to have as great an influence compared to SoyF.

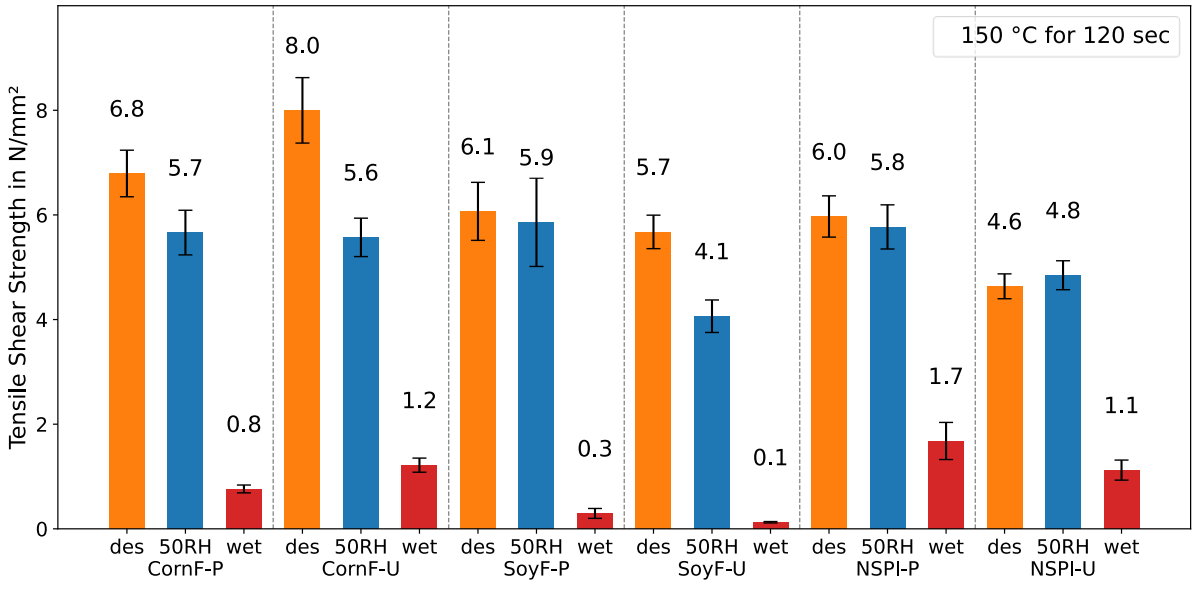

Figure 11: Tensile shear strength of CornF, SoyF and NSPI in P-buffer (P) and in U-buffer (U), tested dry after storage for one day in a desiccator (des), tested dry after storage for one day at 21 °C and 50 % relative humidity (50RH) and tested wet after storage for one day at 21 °C and 50 % relative humidity and soaking in water for four hours (wet).

4.3. Complex viscosity

Figure 12 shows images of high-concentration samples of CornF, SoyF and NSPI. Based on the results of Figure 13, the viscosity was very different in some cases. The complex viscosity of CornF increased considerably with the addition of urea. The differences between SoyF and NSPI were not as pronounced. In addition, a gel-like structure was formed for NSPI-U with increasing settling time.

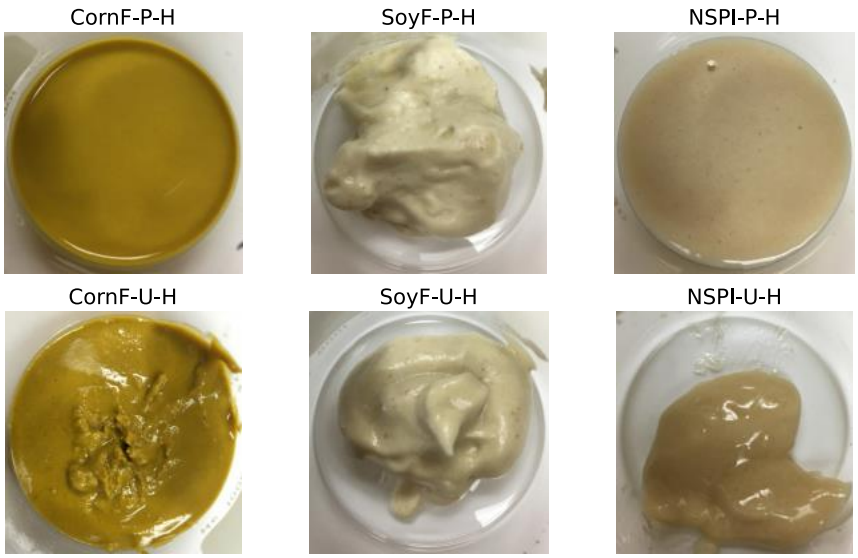

Figure 12: High-concentration (H) samples of CornF, SoyF and NSPI in P-buffer (P) and U-buffer (U).

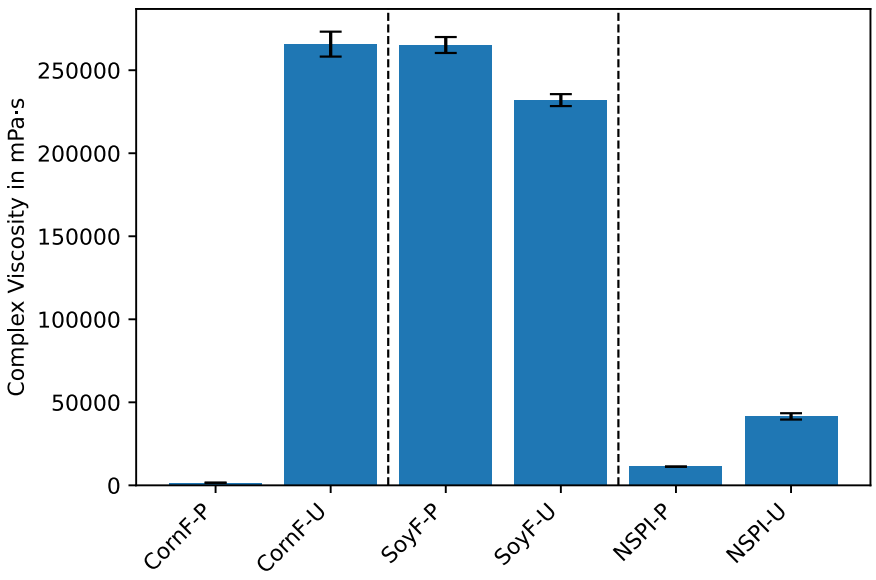

Figure 13: Complex Viscosity of CornF, SoyF and NSPI in P-buffer (P) and U-buffer (U).

4.4. Particle characterization via light scattering

4.4.1. DLS

The hydrodynamic diameter results of our proteins indicated that the presence of urea caused larger diameters for all proteins (Figure 14). CornF exhibited the highest hydrodynamic diameter of 907.3 nm in the U-buffer and the second-highest value of 398.8 in the P-buffer. Conversely, the lowest values were measured for SoyF and NSPI in the P-buffer, with dimensions of 38.9 nm and 41.2 nm in the backscattering mode. A significant difference in particle size was observed between CornF-P-90° and SoyF-P-Back or NSPI-P-Back, as well as between CornF-U-90° and the same two samples measured in backscattering mode, indicating a distinct particle size between CornF and the two soy proteins in the P-buffer.

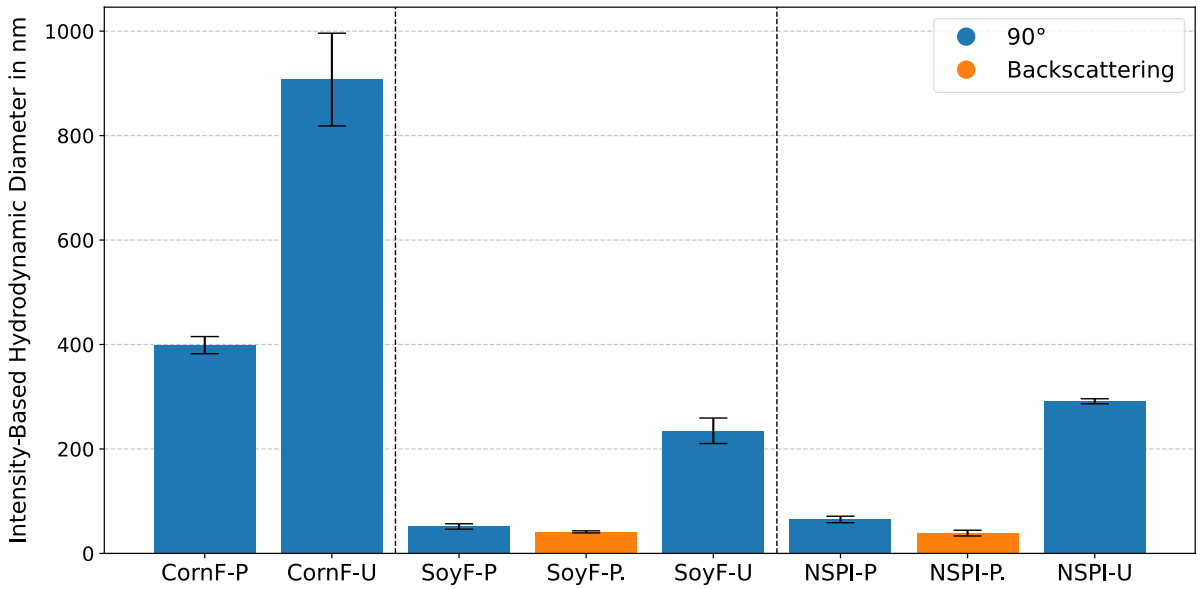

Figure 14: Hydrodynamic Diameter of the supernatant of CornF, SoyF, and NSPI in P-buffer (P) and in U-buffer (U), in the 90° and backscattering measuring mode. If the Hydrodynamic Diameter was approximately 50 nm in the 90° measuring mode, replicates in the backscattering mode were measured.

In addition, intensity- (Figure 15) and volume-based probability distributions (Figure 16) were plotted due to the polydispersity of our samples. In Figure 15 one can see hints of two peaks for almost all samples, which are not visible in Figure 16, as the weighting of larger particles is greater in the intensity-based analysis than in the volume-based one. Due to the lower contribution of larger particles in the backscattering mode, the "second peak" disappeared with a larger particle diameter, especially with the volume-based backscattering measurements, but also with SoyF-P-90° and NSPI-P-90°. For CornF-U-90°, SoyF-U-90° and NSPI-U-90°, it appeared that the distribution remained almost the same and only the values

of the probability distribution got lower. CornF-P-90° seemed to have a larger proportion of medium-sized particles, which did not contribute much to the probability distribution in terms of volume.

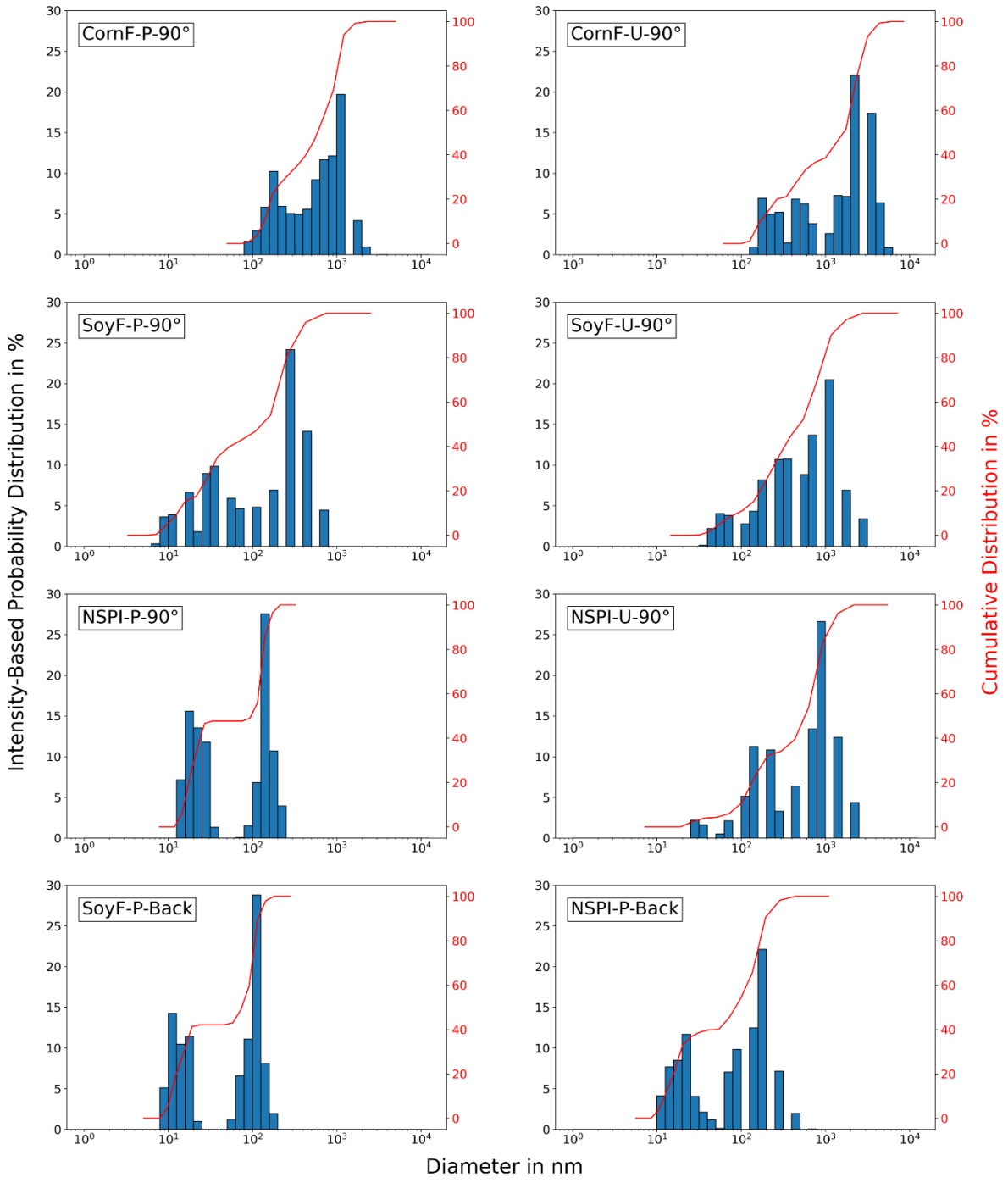

Figure 15: Intensity-Based Probability Distribution of the supernatant of CornF, SoyF and NSPI samples in P-buffer (P) and in U-buffer (U) at low concentrations in the 90° and backscattering mode.

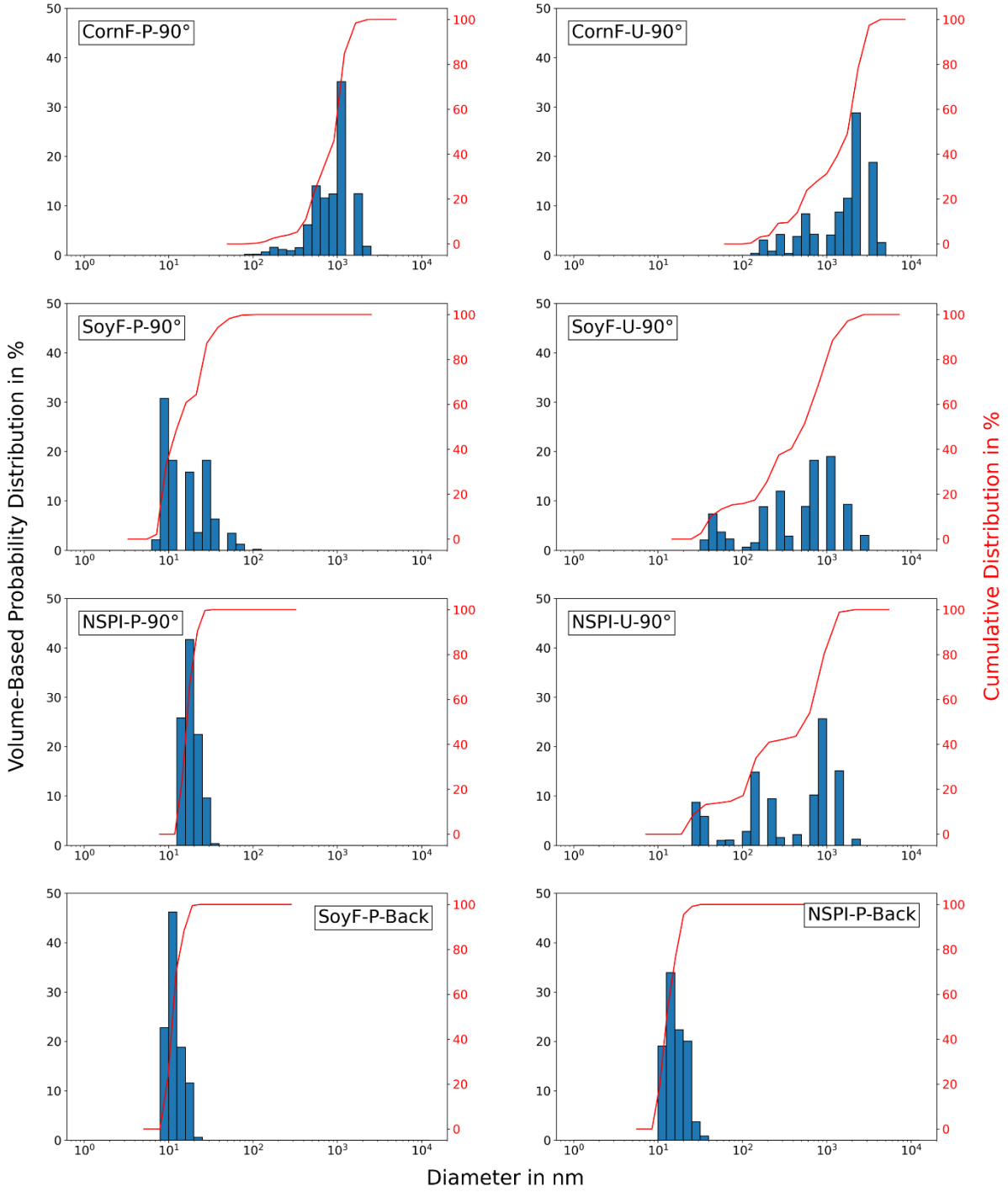

Figure 16: Volume-Based Probability Distribution of the supernatant of CornF, SoyF and NSPI samples in P-buffer (P) and in U-buffer (U) at low concentrations in the 90° and backscattering mode.

4.4.2. MALS

Without specifying a particular shape, $R_{g\ Guinier}$ exhibited similar values across all samples (Table 2). Generally, CornF displayed slightly higher values, consistent with the DLS data results. Additionally, values were elevated for CornF and SoyF in the U-buffer compared to the P-buffer samples, with NSPI showing the opposite trend. By analyzing the ratio of the fitted $R_{g\ Guinier}$ values to the hydrodynamic radius from DLS measurements, it was observed that all values, except for SoyF-P and NSPI-P, were below 0.8, indicative of a solid sphere shape. Values for SoyF and NSPI in P-buffer were approximately twice as high as what would be expected for an extended rod shape, which would be 1.6. Contributions from carbohydrates and other substances could have potentially interfered with the analyzed ratio. Additionally, the absence of a cut-off for the MALS data meant that contributions from dust particles could have also impacted the results. Nevertheless, considering the data, it's improbable that urea causes a shape of an extended rod, since the ratio of all proteins in U-buffer had values lower than 0.8.

Table 3 presents the outcomes of the fitting process using a polydisperse sphere and cylinder model. Focusing on the results of the sphere fit, it was evident that the presence of urea consistently leads to an increase in radius of the soluble part of the proteins. CornF exhibited larger radii compared to SoyF and NSPI, both having roughly the similar size. Examining the results of the cylinder model, the data for CornF in both P-buffer and U-buffer indicated a fit of a compressed cylindrical shape, resembling more the form of a sphere that is not exactly spherical. On the other hand, the fit obtained for SoyF and NSPI in both P-buffer and U-buffer suggested a more extended cylindrical shape.

Table 2: Radius of gyration fitted with a Guinier plot ($R_{g\ Guinier}$) and ratio of $R_{g\ Guinier}$ to R_h for CornF, SoyF and NSPI in P-buffer (P) and U-buffer (U). $R_{g\ Guinier}$ / R_h = 1.6 → extended rod, $R_{g\ Guinier}$ / R_h = 0.8 → solid sphere.

Sample description	**$R_{g\ Guinier}$ in nm**	**$R_{g\ Guinier}$ / R_h**
CornF-P	84.0	0.4
CornF-U	108.9	0.2
SoyF-P	65.9	3.4
SoyF-U	70.8	0.5
NSPI-P	65.5	3.2
NSPI-U	54.5	0.5

Table 3: Fitted radius (R) and length (L) of a polydisperse sphere and cylinder model for CornF, SoyF and NSPI in P-buffer (P) and U-buffer (U).

Sample description	R in nm	L in nm
CornF-P-Sph	138.2	-
CornF-U-Sph	237.5	-
CornF-P-Cyl	435.9	148.2
CornF-U-Cyl	149.2	589.4
SoyF-P-Sph	86.7	-
SoyF-U-Sph	113.0	-
SoyF-P-Cyl	43.7	776.0
SoyF-U-Cyl	399.3	89.1
NSPI-P-Sph	95.0	-
NSPI-U-Sph	106.9	-
NSPI-P-Cyl	63.1	4634.7
NSPI-U-Cyl	5177.6	60.9

To determine the likelihood of the models, the R_g values from both the sphere and cylinder models, as well as the Guinier fit, have been summarized in Table 4. The ratios of these values to the hydrodynamic radius are also listed. Upon examining the R_g values, it was observed that the R_g values from the Guinier fit, which assumed no specific shape, were similar to those from the sphere model. The R_g values from the cylinder model were higher compared to the values from the Guinier fit, reinforcing the assumption that, even in the presence of urea, all particles are more likely to have a spherical shape than a cylindrical one. The comparison of the ratios further supports this assertion.

Table 4: Comparison of $R_{g\ Sph}$, $R_{g\ Cyl}$ and $R_{g\ Guinier}$, as well of $R_{g\ Sph}$ / R_h, $R_{g\ Cyl}$ / R_h and $R_{g\ Guinier}$ / R_h.

Sample description	**$R_{g\ Sph}$ in nm**	**$R_{g\ Cyl}$ in nm**	**$R_{g\ Guinier}$ in nm**	**$R_{g\ Sph}$ / R_h**	**$R_{g\ Cyl}$ / R_h**	**$R_{g\ Guinier}$ / R_h**
CornF-P-Sph	107.0	-	84.0	0.5	-	0.4
CornF-U-Sph	183.9	-	108.9	0.4	-	0.2
CornF-P-Cyl	-	311.2	84.0	-	1.6	0.4
CornF-U-Cyl	-	200.2	108.9	-	0.4	0.2
SoyF-P-Sph	67.2	-	65.9	3.5	-	3.4
SoyF-U-Sph	87.5	-	70.8	0.6	-	0.5
SoyF-P-Cyl	-	225.3	65.9	-	11.6	3.4
SoyF-U-Cyl	-	220.2	70.8	-	1.5	0.5
NSPI-P-Sph	73.6	-	65.5	3.6	-	3.2
NSPI-U-Sph	82.8	-	54.5	0.7	-	0.5
NSPI-P-Cyl	-	1338.4	65.5	-	65.0	3.2
NSPI-U-Cyl	-	2835.9	54.5	-	24.2	0.5

5. Discussion

In this study, we explored different methodologies designed to detect structural changes in proteins induced by the presence of urea. The aim was to determine the impact of these effects on coalescence of proteins and protein adhesive strength. Our findings indicated that potentially a higher hydrophobic content in CornF correlates with increased wet strength values. Additionally, employing diverse methods allowed us to identify certain trends in CornF, SoyF, and NSPI, suggesting that all proteins retain a spherical shape even in the presence of urea and the protein diameters increases due to the urea exposure.

Based on deconvolution of fluorescence measurements into three different peaks, a clear hydrophobic peak could be recognized for CornF, which was not apparent for either soybean-based samples or tryptophan. Corn is generally known to have a higher proportion of non-polar amino acids, specifically leucine, alanine, and proline, which are constituents of the predominant storage protein, zein. In contrast, soy protein is predominantly composed of 90 % globulins, specifically glycinin and conglycinin, both exhibiting a polar nature (Dunky, 2021). Due to the presence of two peaks in the fluorescence spectra of CornF, these spectra were not analyzed for a peak shift and KI quenching. However, it was noted that only the more hydrophilic portion experienced a reduction in intensity when KI was added. This aligns with the hypothesis that hydrophilic tryptophan residues near the surface of a protein can be quenched since they are readily accessible to the solvated quenching agent, KI. In contrast, hydrophobic tryptophan residues are unaffected because the quencher is unable to reach them due to the conformational arrangement of surrounding amino acids (Atkins & Paula, 2006; E. A. Burstein et al., 1973). In the context of KI quenching with SoyF and NSPI, a blue shift appeared with increasing KI concentration, highlighting the multi-component nature of the protein's emission spectrum (Reshetnyak & Burstein, 2001). Furthermore, our results for SoyF and NPSI showed that there is a general peak shift towards longer wavelengths and therefore a higher portion of tryptophan residues in a hydrophilic environment due to the presence of urea. This trend is often interpreted in the literature as an unfolding of the protein in both isolates and flour (Cheng et al., 2004; Creighton, 1979; Scholtz et al., 1995). However, stating this claim is quite bold because fluorescence data alone doesn't provide a complete picture of how protein structure changes to increase tryptophan accessibility. Estimations about the extent of this accessibility can be made, but a more thorough understanding of the structural changes requires a holistic approach.

Tensile shear strength measurements revealed differences between CornF, SoyF, and NSPI samples. Wet strength comparison between SoyF and NSPI revealed a lower strength in SoyF. Given that flours consist approximately 50 - 40 % of non-protein components, which are

mainly carbohydrates, this outcome was anticipated, as these components typically do not contribute to increase strength values (Lorenz et al., 2015). Interestingly, however, wet strength of CornF was higher than that of SoyF. CornF in general contained a higher proportion of hydrophobic amino acids than the soy samples and Kallakas et al. (2024) found a direct correlation between wet strength and surface hydrophobicity. Furthermore, CornF exhibited higher strength values after one day in the desiccator compared to under storage conditions with higher relative humidity, suggesting that lower humidity contributed to its superior strength. In general, protein's expansion is expected to enhance wet strength through increased protein-protein interactions and improved film coalescence. Conversely, the addition of urea to SoyF and NSPI reduced strength values. Although urea likely weakened strength by reducing protein-protein interaction strength, its water solubility facilitated removal during water soak, allowing proteins to interact. However, there was clearly no large boost in strength resulting from enhanced protein interactions that might have been expected from extended proteins. To summarize the ABES results, it can be assumed that a higher proportion of protein correlated with higher strength values, and CornF, which contained more hydrophobic compounds, exhibited increased wet strength, even with a higher proportion of non-protein components present.

The increase in complex viscosity observed in CornF when exposed to urea, as opposed to minimal changes in NSPI and the opposite effect in SoyF, could be attributed to several reasons. One possible explanation is the aggregation of proteins, which can happen in highly concentrated samples due to electrostatic forces, van der Waals forces, hydration effects, hydrophobic interactions, and steric influences (Bauer et al., 2017). Additionally, urea also tends to aggregate in water, as indicated by concentration and temperature dependent trends observed through dynamic light scattering (Atahar et al., 2019). The combined effect of a higher proportion of hydrophobic amino acids in CornF compared to the soy samples, along with the fact that urea aggregates in water, could explain the higher complex viscosity of CornF in the presence of urea. SoyF and NSPI could possibly contain components that do not promote the aggregation of proteins as strongly and therefore the influence of urea was not as pronounced, at least in the case of NSPI. In addition, minor viscosity changes upon urea addition to soy suggest limited protein swelling.

Light scattering results supported the statement that urea leads to a kind of aggregation of the proteins. Two different methods (DLS and MALS) were used to detect an increase in size due to the presence of urea. In contrast to the literature, our data could not support the assumption that urea leads to an extended form and thus denatures the proteins, which should lead to higher strength values. On the contrary, our results indicated that for all proteins a spherical shape is more plausible than a cylindrical one and just the size of the particles is

increasing via aggregation in the presence of urea. If the proteins were to swell in urea, solvent would be required to fill the voids created inside the loose protein structure, increasing the volume fraction of “solid” proteins. Based on the extremely steep solids vs viscosity curve of soy in this region (Frihart & Gargulak, 2022), we expect significant swelling of the proteins, even increasing in volume by 20 %, would cause orders of magnitude increases in viscosity.

6. Conclusion

We were able to disprove the widespread assumption that urea, as a denaturant, extends soy proteins, exposing dramatically more amino acid residues to the solvent. It is expected that this expansion of the protein would lead to protein-protein interactions, greater entanglement of the protein polymers and better coalescence of the protein film, which in turn would result in better wet strength. On the contrary, the addition of urea to SoyF and NSPI led to a reduction in strength values. The opposite was observed for CornF, but it is more likely that its higher hydrophobic content and larger initial particle size led to higher wet and dry strength from CornF samples with a low moisture content. Both SoyF and CornF are cheaper alternatives to protein isolates because both are by-products of starch or soybean oil production. Protein isolates require an additional production step to increase the protein content. Comparing the flours, CornF showed great potential compared to SoyF, as higher wet strengths could be achieved. NSPI achieved the highest or equally good wet strength as CornF presumably due to a higher degree of purity or relative protein content. In addition, for all proteins it could be shown that a spherical shape was more likely than a cylindrical one and that urea only increased the diameter of the particles, which indicated that there is likely aggregation of primary particles. Fluorescence data showed that the structure of all proteins changed only to the extent that the amino acid tryptophan was more accessible when urea was present in the solution. The reason for this is still undecided. Perhaps the aggregation of urea with the proteins loosened their structure, increasing the accessibility of tryptophan at the same time. In conclusion, corn flour is a good alternative for industrial applications compared to soy flour, which has been the most widely used so far. However, modifications are still required to meet the requirements of commercial products.

7. References

Akbar, S. M., Sreeramulu, K., & Sharma, H. C. (2016). Tryptophan fluorescence quenching as a binding assay to monitor protein conformation changes in the membrane of intact mitochondria. *Journal of Bioenergetics and Biomembranes*, *48*(3), 241–247. https://doi.org/10.1007/s10863-016-9653-0

AOCS (2017a). *Protein Dispersibility Index:* Standard procedure Ba 10b-09.

AOCS (2017b). *Urease Activity:* Official Method Ba 9-58.

ASTM International (2019). *Standard Test Method for Measuring the Effect of Temperature on the Cohesive Strength Development of Adhesives using Lap Shear Bonds under Tensile Loading* (D7998-19).

Atahar, A., Mafy, N. N., Rahman, M. M., Mollah, M. Y. A., & Susan, M. A. B. H. (2019). Aggregation of urea in water: Dynamic light scattering analyses. *Journal of Molecular Liquids*, *294*, 111612. https://doi.org/10.1016/j.molliq.2019.111612

Atkins, P. W., & Paula, J. de. (2006). *Physical chemistry* (8th ed.). W.H. Freeman.

Averina, E., Konnerth, J., D'Amico, S., & van Herwijnen, H. W. (2021). Protein adhesives: Alkaline hydrolysis of different crop proteins as modification for improved wood bonding performance. *Industrial Crops and Products*, *161.* https://doi.org/10.1016/j.indcrop.2020.113187

Averina, E., Konnerth, J., & van Herwijnen, H. W. (2023). Protein-based glyoxal–polyethyleneimine-crosslinked adhesives for wood bonding. *The Journal of Adhesion*, *99*(3), 363–378. https://doi.org/10.1080/00218464.2021.2020111

Barer, R., Ross, K. F. A., & Tkaczyk, S. (1953). Refractometry of living cells. *Nature*, *171*(4356), 720–724. https://doi.org/10.1038/171720a0

Bauer, K. C., Suhm, S., Wöll, A. K., & Hubbuch, J. (2017). Impact of additives on the formation of protein aggregates and viscosity in concentrated protein solutions. *International Journal of Pharmaceutics*, *516*(1-2), 82–90. https://doi.org/10.1016/j.ijpharm.2016.11.009

Brookhaven Instruments. (2024). *The NanoBrook Series is a Configurable Platform for Particle Sizing and Zeta Potential Measurements.* Brookhaven Instruments. https://www.brookhaveninstruments.com/product/nanobrook-series/

Burstein, E. A., Vedenkina, N. S., & Ivkova, M. N. (1973). Fluorescence and the location of tryptophan residues in protein molecules. *Photochemistry and Photobiology*, *18*(4), 263–279. https://doi.org/10.1111/j.1751-1097.1973.tb06422.x

Burstein, E., & Emelyanenko, V. I. (1996). Log-Normal Description of Fluorescence Spectra of Organic Fluorophores. *Photochemistry and Photobiology*, *64*(2), 316–320. https://doi.org/10.1111/j.1751-1097.1996.tb02464.x

Cemin, H. S., Tokach, M. D., Dritz, S. S., Woodworth, J. C., DeRouchey, J. M., Goodband, R. D., & Wilken, M. (2019). Evaluating the Productive Energy Content of High-Protein Distillers Dried Grains in Swine Diets. *Kansas Agricultural Experiment Station Research Reports*, *5*(8). https://doi.org/10.4148/2378-5977.7852

Cheng, E., Sun, X., & Karr, G. S. (2004). Adhesive properties of modified soybean flour in wheat straw particleboard. *Composites Part a: Applied Science and Manufacturing*, *35*(3), 297–302. https://doi.org/10.1016/j.compositesa.2003.09.008

Creighton, T. E. (1979). Electrophoretic analysis of the unfolding of proteins by urea. *Journal of Molecular Biology*, *129*(2), 235–264. https://doi.org/10.1016/0022-2836(79)90279-1

Damodaran, S. (2017). *Food proteins and their applications* (First edition). *Food Science and Technology: Vol. 80*. Taylor and Francis. https://permalink.obvsg.at/

Dunky, M. (2021). Wood Adhesives Based on Natural Resources: A Critical Review: Part I. Protein-based Adhesives. In K. L. Mittal (Ed.), *Progress in adhesion and adhesives* (pp. 203–336). Scrivener Publishing; Wiley. https://doi.org/10.1002/9781119846703.ch8

FAO (2019). Global forest products facts and figures 2018.

Frihart, C. R., & Gargulak, M [Matthew] (2022). Use of Dynamic Shear Rheology to Understand Soy Protein Dispersion Properties. *Polymers*, *14*(24). https://doi.org/10.3390/polym14245490

Frihart, C. R., Hunt, C. G., & Birkeland, M. J. (2013). Soy Proteins as Wood Adhesives. In W. Gutowski & H. Dodiuk (Eds.), *Recent Advances in Adhesion Science and Technology in Honor of Dr. Kash Mittal* (pp. 283–304). CRC Press. https://doi.org/10.1201/b16347-21

Gandhi, S. (2002). Effect of pH and temperature on conformational changes of a humanized monoclonal antibody.

Glatter, O. (Ed.). (1983). *Small angle X-ray scattering* (2. print). Academic Press.

Huang, W., & Sun, X. (2000). Adhesive properties of soy proteins modified by urea and guanidine hydrochloride. *Journal of the American Oil Chemists' Society*, *77*(1), 101–104. https://doi.org/10.1007/s11746-000-0016-6

Hunt, C. G., Lorenz, L. F., Houtman, C. J., Valle, E., Coolidge, T., Mock, C., & Frihart, C. R. (2022). Jet cooking dramatically improves the wet strength of soy adhesives. *Journal of the American Oil Chemists' Society*, *100*(1), 69–79. https://doi.org/10.1002/aocs.12664

Kallakas, H., Plaza, N., Crooks, C., Turner, D., Gargulak, M [Mathew], Arvanitis, M. A., Frihart, C. R., & Hunt, C. G. (2024). Effect of Protein Surface Hydrophobicity and Surface Amines on Soy Adhesive Strength. *Polymers*, *16*(2). https://doi.org/10.3390/polym16020202

Lásztity, R. (1996). *The chemistry of cereal proteins* (2nd ed.). CRC Press. http://www.loc.gov/catdir/enhancements/fy0744/95022630-d.html

Lehrer, S. S. (1971). Solute perturbation of protein fluorescence. Quenching of the tryptophyl fluorescence of model compounds and of lysozyme by iodide ion. *Biochemistry*(10), Article 17.

Liu, K. (1997). *Soybeans: Chemistry, Technology, and Utilization*. Springer US. https://doi.org/10.1007/978-1-4615-1763-4

Lorenz, L., Birkeland, M., Daurio, C., & Frihart, C. R. (2015). Soy Flour Adhesive Strength Compared with That of Purified Soy Proteins *Forest Products Journal*, *65*(1-2), 26–30. https://doi.org/10.13073/FPJ-D-13-00020

Malvern Instruments Limited (2017). Dynamic Light Scattering: An Introduction in 30 Minutes.

Niemz, P., Teischinger, A., & Sandberg, D. (2023). *Springer Handbook of Wood Science and Technology*. Springer International Publishing. https://doi.org/10.1007/978-3-030-81315-4

Nobbmann, U. (2017). *Intensity-Volume-Number: Which size is correct?* https://www.materials-talks.com/intensity-volume-number-which-size-is-correct/

Pizzi, A., & Mittal, K. L. (2003). *Handbook of adhesive technology* (2nd ed., rev. and expanded.). M. Dekker.

Reshetnyak, Y. K., & Burstein, E. A. (2001). Decomposition of protein tryptophan fluorescence spectra into log-normal components. Ii. The statistical proof of discreteness of tryptophan classes in proteins. *Biophysical Journal*, *81*(3), 1710–1734. https://doi.org/10.1016/S0006-3495(01)75824-9

Reshetnyak, Y. K., Koshevnik, Y., & Burstein, E. A. (2001). Decomposition of protein tryptophan fluorescence spectra into log-normal components. Iii. Correlation between fluorescence and microenvironment parameters of individual tryptophan residues. *Biophysical Journal*, *81*(3), 1735–1758. https://doi.org/10.1016/S0006-3495(01)75825-0

Scholtz, J. M., Barrick, D., York, E. J., Stewart, J. M., & Baldwin, R. L. (1995). Urea unfolding of peptide helices as a model for interpreting protein unfolding. *Proceedings of the National Academy of Sciences of the United States of America*, *92*(1), 185–189. https://doi.org/10.1073/pnas.92.1.185

STATISTA. (2023). *Global corn production in 2022/2023, by country*. https://www.statista.com/statistics/254292/global-corn-production-by-country/

Stetefeld, J., McKenna, S. A., & Patel, T. R. (2016). Dynamic light scattering: A practical guide and applications in biomedical sciences. *Biophysical Reviews*, *8*(4), 409–427. https://doi.org/10.1007/s12551-016-0218-6

Sze, C. K. W., Kshirsagar, H. H., Venkatachalam, M., & Sathe, S. K. (2007). A circular dichroism and fluorescence spectrometric assessment of effects of selected chemical denaturants on soybean (Glycine max L.) storage proteins glycinin (11S) and beta-conglycinin (7S). *Journal of Agricultural and Food Chemistry*, *55*(21), 8745–8753. https://doi.org/10.1021/jf071364e

Vnučec, D., Kutnar, A., & Goršek, A. (2017). Soy-based adhesives for wood-bonding – a review. *Journal of Adhesion Science and Technology*, *31*(8), 910–931. https://doi.org/10.1080/01694243.2016.1237278

Warren, J. R., & Gordon, J. A. (1966). On the Refractive Indices of Aqueous Solutions of Urea. *The Journal of Physical Chemistry*, *70*(1), 297–300. https://doi.org/10.1021/j100873a507

Wyatt, P. J. (1997). Multiangle Light Scattering: The Basic Tool for Macromolecular Characterization. *Instrumentation Science & Technology*, *25*(1), 1–18. https://doi.org/10.1080/10739149709351443

Zhang, B., Wang, J., Zhang, F., Wu, L., Guo, B., Gao, Z., & Zhang, L. (2022). Preparation of a High-Temperature Soybean Meal-Based Adhesive with Desired Properties via Recombination of Protein Molecules. *ACS Omega*, *7*(27), 23138–23146. https://doi.org/10.1021/acsomega.2c00833

Zhang, Y., Zhang, M., Chen, M., Luo, J., Li, X., Gao, Q., & Li, J. (2018). Preparation and characterization of a soy protein-based high-performance adhesive with a hyperbranched cross-linked structure. *Chemical Engineering Journal*, *354*, 1032–1041. https://doi.org/10.1016/j.cej.2018.08.072

Zhang, Z., & Hua, Y. (2007). Urea-Modified Soy Globulin Proteins (7S and 11S): Effect of Wettability and Secondary Structure on Adhesion. *Journal of the American Oil Chemists' Society*, *84*(9), 853–857. https://doi.org/10.1007/s11746-007-1108-7

List of tables

List of figures

Appendix

Table 5: Amino acid composition of soybean flour and corn (Cemin et al., 2019).

Amino acid	Soybean flour	Relative amount	Corn	Relative amount
Alanine	2.01	4.39	0.56	7.45
Arginine	3.38	7.38	0.37	4.92
Aspartic acid	5.27	11.51	0.53	7.05
Cysteine	0.7	1.53	0.19	2.53
Glutamic acid	8.48	18.52	1.39	18.48
Glycine	2	4.37	0.31	4.12
Histidine	1.2	2.62	0.22	2.93
Isoleucine	2.27	4.96	0.28	3.72
Leucine	3.58	7.82	0.88	11.70
Lysine	3.01	6.57	0.27	3.59
Methionine	0.66	1.44	0.18	2.39
Phenylalanine	2.38	5.20	0.38	5.05
Proline	2.37	5.17	0.67	8.91
Serine	2.01	4.39	0.34	4.52
Threonine	1.81	3.95	0.28	3.72
Tryptophan	0.63	1.38	0.06	0.80
Tyrosine	1.72	3.76	0.23	3.06
Valine	2.32	5.07	0.38	5.05